Int. J. Electrochem. Sci., 14 **(2019)** 7703 – 7716, doi: 10.20964/2019.08.42

International Journal of
ELECTROCHEMICAL
SCIENCE
www.electrochemsci.org

Facile Synthesis of Fe-MOF/rGO nanocomposite as an Efficient Electrocatalyst for Nonenzymatic H_2O_2 Sensing

Suling Yang[1,2,*], *Mengyu Li*[1,2], *Ziling Guo*[1,2], *Ning Xia*[1,2,*], *Lingbo Qu* [1,3]

[1] College of Chemistry and Chemical Engineering, Anyang Normal University, Anyang 455002, PR China
[2] Henan Key Laboratory of New Opto-electronic Functional Materials
[3] College of Chemistry and Molecular Engineering, Zhengzhou University, Zhengzhou 450001, PR China
[*]E-mail: yang_suling@163.com; xianing82414@163.com

Received: 17 March 2019 / *Accepted:* 15 May 2019 / *Published:* 30 June 2019

An Fe-MOF (metal−organic framework)/reduce graphene oxide (rGO) nanocomposite was formed by using an efficient synthetic method. The morphology and structure of the Fe-MOF/rGO nanocomposite were characterized by scanning electron spectroscopy (SEM) and X-ray diffraction (XRD). The Fe-MOF/rGO nanocomposites were immobilized on a carbon paste electrode (CPE) to construct a high-performance nonenzymatic electrochemical H_2O_2 sensor. A cyclic voltammetry (CV) study showed that the Fe-MOF/rGO nanocomposites displayed better electrocatalytic activity toward H_2O_2 reduction compared to that of Fe-MOF. An amperometric study indicated that the H_2O_2 sensor displayed high performance, which offered a low detection limit (0.5 μM), a high sensitivity (5.17 μA mM^{-1} cm^{-2}), and a wide linear range (from 5.0 to 945 μM). An electrochemical reaction mechanism was proposed for H_2O_2 reduction on the Fe-MOF/rGO/CPE. Importantly, the as-fabricated H_2O_2 sensor exhibited good reproducibility and excellent selectivity. Furthermore, the constructed high-performance sensor was utilized to monitor the H_2O_2 levels in real samples, and satisfactory results were obtained. These results demonstrated that the Fe-MOF/rGO nanocomposite can be used as a good electrochemical sensor material in practical applications.

Keywords: Metal organic framework, Fe-MOF/rGO nanocomposite, electrocatalytic activity, H_2O_2.

1. INTRODUCTION

In recent years, hydrogen peroxide (H_2O_2) has attracted considerable attention due to its important applications in food, industrial engineering, agriculture, medicine and health, clinical control and the environment [1−3].Thus, it would be very valuable to develop a simple, fast, reliable and accurate technique to detect H_2O_2. Among the various techniques proposed for H_2O_2 monitoring, electrochemical methods are the most convenient and effective [4−6].Unfortunately, the enzyme-based

biosensor for H_2O_2 detection cannot be subjected to harsh environments because enzymes can easily degrade, denature and become inactive after they are applied onto the electrode surface, and enzyme-based biosensors have high costs and storage requirements[7]. To overcome several of the limitations defined above, peroxidase-like nanocomposite-based nonenzymatic electrochemical sensors for H_2O_2 detection have been developed in recent years. To obtain various nanocomposites with peroxidase-like bioactivity, noble metal-based materials (Pt, Pd, Ag, Au, etc.) [8−10],carbon-based composites [11, 12],metal oxide-based composites (MnO_2 [13], ZnO [14], Sn_3O_4 [15], etc.), MOFs [15, 16], etc., have been proposed and constructed to prepare nonenzymatic H_2O_2 sensors. Moreover, MOFs are worth further studying for the preparation of ideal catalytically active nanocomposites [17].

Metal−organic frameworks (MOFs), formed by metal connectors and organic linker molecules through strong coordinating bonds, have attracted enormous attention in recent years due to their advantages of ordered crystalline structures, large pore volumes, highly accessible surface areas, chemical tunability and available metal sites [18]. Owing to these remarkable merits, MOFs have been widely applied in the areas of catalysis, drug delivery, and gas storage [17, 19−21]. Moreover, MOFs and their derived nanomaterials are interesting electrode materials and have been used in solar cells, energy storage devices, lithium-ion rechargeable batteries, fuel cells, and sensors [22−24]. Nevertheless, the few adverse properties of MOFs are their poor thermal stability, weak electrical conductivity, and low mechanical strength and unstable nature in aqueous solution, which limit their further use as electrochemical sensors. In recent years, high-conductivity materials (carbon–based materials, noble metal-based materials, transition metal-based materials, etc.) have been coupled with MOFs to form nanocomposites and improve the electrochemical properties and electron conductivities of MOFs [25−27]. The utilization of MOFs as a component in the preparation of metal-MOF/graphene-based materials is a convenient and effective strategy to enhance the electrochemical performance of MOFs [1, 4].

Graphene, a single layer of carbon atoms in a two-dimensional lattice, has received widespread attention due to its interesting nanostructure and extraordinary properties, such as high electron conductivity and exceptionally high surface area. These excellent properties make graphene a promising component for the preparation of graphene-MOF composites to enhance the electrochemical performance of MOFs. In recent years, many techniques have been developed to prepare graphene-MOF composites, including in situ growth, hydrothermal, direct mixing, Pickering emulsion polymerization, and atomic layer deposition methods [28−30]. However, the above-mentioned methods still have shortcomings regarding the scalability and controllability of the preparation process for graphene−MOF composites. The strategy of directly mixing MOFs with graphene has been widely applied for obtaining graphene−MOF composites [31, 32], but the preparation process often suffers from the following problems. The addition of the MOF components may not effectively prevent the aggregation of graphene nanosheets, which normally results in an uneven dispersion of each of the components within the resulting graphene−MOF composite. Although several researchers [33, 34] have reported that 3D graphene structures can be applied as templates for the production of graphene−MOF composites with uniform hierarchical structures, complex synthetic steps are normally required. Thus, it is still challenging to develop a low-cost, high-dimensionally controllable and

convenient synthesis for graphene−MOF composites.

In this research, chitosan (CS) was used to reduce graphene oxide (GO) into reduced GO (rGO) and introduce functional groups (−NH_2, −COOH) onto the surface of rGO. In addition, CS enables rGO to be well dispersed in an aqueous solution. Subsequently, functionalized rGO is an ideal support material for Fe-MOFs. We proposed a general, simple, and inexpensive approach, called the simple mixing method, for the preparation of Fe-MOF/rGO nanocomposites, which can be used as electrode-modifying materials. The prepared Fe-MOF/rGO nanocomposite, derived from a Fe-MOF and graphene, exhibited excellent electrochemical performance for the application of nonenzymatic detection of H_2O_2.

2. EXPERIMENTAL

2.1 Reagents and solutions

Ultrapure water was obtained from a Millipore Milli-Q UF-Plus Ultrapure Water System (Mequon, WI US) (18 MΩ · cm) and used throughout the experiments unless otherwise noted. H_2O_2 (30% w/w in H_2O), p-phthalic acid, $FeCl_3$, glucose, ethanol, uric acid (UA), ascorbic acid (AA), graphite power (99.95%, 325 mesh), CS (75% deacetylated) and N,N-dimethylformamide (DMF) were purchased from Sigma-Aldrich and used as received. All other chemicals used were of at least analytical reagent grade. A CS solution (0.5 wt%) was prepared by dissolving CS powder in an acetic acid (1 wt%) solution and then adjusting the pH to 5~6. The prepared CS solution was stored in a refrigerator until used. A 0.1 M pH 7.0 phosphate buffered saline (PBS) solution was used for H_2O_2 detection. All solutions were deoxygenated by purging with nitrogen gas before use.

2.2 Apparatus

A CHI 842C electrochemical workstation (Austin, TX, USA) was used to perform the electrochemical experiments. A conventional three-electrode system was used, in which either a bare CPE or modified CPE was used as the working electrode, Ag/AgCl (saturated KCl) and a platinum wire were used as the reference and counter electrodes, respectively. The potentials measured during the electrochemical experiments refer to this reference electrode. The surface morphology was characterized using field emission scanning electron microscopy (FESEM, JEOL 7401 F) and an X-ray diffractometer (Philips, X'pert, Netherland).

2.3 Synthesis of the Fe-MOF

The Fe-MOF was synthesized by reacting the precursor mixture at 100 °C according to a previously reported protocol with minor changes [35]. Briefly, a solid mixture of $FeCl_3$ and p-phthalic acid was prepared with a weight ratio of 1.5:1 in DMF and then stirred to obtain a uniform solution at room temperature. Subsequently, the as-obtained solution was transferred into a high-temperature and

high-pressure autoclave and subjected to hydrothermal reduction at 100 °C for 12 h. Afterward, the resulting orange-red precipitate was collected by centrifugation and washed with anhydrous ethanol. Finally, the purified precipitate was dried at 30 °C for vacuum drying, and the Fe-MOF was obtained for further characterization and preparation of the sensor.

2.4 Preparation of a H_2O_2 biosensor

GO was prepared according to a modified Hummers method [36]. Subsequently, rGO was obtained using CS as a reductant to reduce GO. In brief, equivalent volumes of 1 mg/mL GO and 0.5 wt% CS solutions were stirred until a uniform yellow-brown solution was achieved. Subsequently, the above-mentioned solution was placed in a 90 ºC water bath accompanied by vigorous stirring for 5 h until the color of the solution turned black. Finally, the resulting product was centrifuged and washed 3 times to obtain the CS-functionalized rGO. The properties of the synthesized rGO were consistent with those documented in previous reports [4, 37]. The detailed characterization results and discussion of the CS-rGO are shown in Figure S1.

The Fe-MOF/rGO composite was prepared through a simple mixing method. Briefly, the prepared Fe-MOF crystals (30 mg) were rapidly added into a methanol dispersion of graphene (1 mg/mL, 20 mL) under vigorous sonication to form an Fe-MOF/rGO suspension. Afterwards, the prepared composite suspension was subjected to a freeze-dry process to remove methanol and obtain an Fe-MOF/rGO composite powder. A bare CPE was prepared by mixing spectral graphite and silicone oil in a mass ratio of 80:30. The paste was thoroughly hand-mixed in a mortar and then firmly pressed into one end of a glassy tube (d = 4 mm). Electrical contact was established by a copper wire inserted deep into the opposite end of the tube. For electrode modification, 2 mg of the Fe-MOF/rGO powder was dispersed into 1 mL of N,N-dimethylformamide by sonication. A 6.0 μL aliquot of the Fe-MOF/rGO suspension was drop cast onto the CPE to form the Fe-MOF/CS-rGO-modified CPE (Fe-MOF/rGO/CPE). For comparison, an Fe-MOF/CPE and rGO/CPE were prepared through a similar procedure.

3. RESULTS AND DISCUSSION

3.1 Morphology and physical characterization of the Fe-MOF

The characterizations of rGO are shown in Figure S1 (Supporting Information). The morphologies of the prepared Fe-MOF and the Fe-MOF/rGO composite (the weight ratio of Fe-MOF to rGO is 3:2) are shown in Figure 1. The obtained Fe-MOF (Figure 1a) crystals exhibit a highly regular six-angle bipyramidal structure. Moreover, Fe-MOF crystals with a size of approximately 400 nm can be clearly observed. The SEM image of the Fe-MOF/rGO composite shows several wrinkled and folded sheets (Figure 1b), indicating the presence of rGO sheets. The Fe-MOF crystals that are uniformly mixed with the rGO nanosheets have a morphology similar to that of the pristine Fe-MOF crystals, which is consistent with the observations shown in Figure 1a, further confirming the formation of the Fe-MOF/rGO composite.

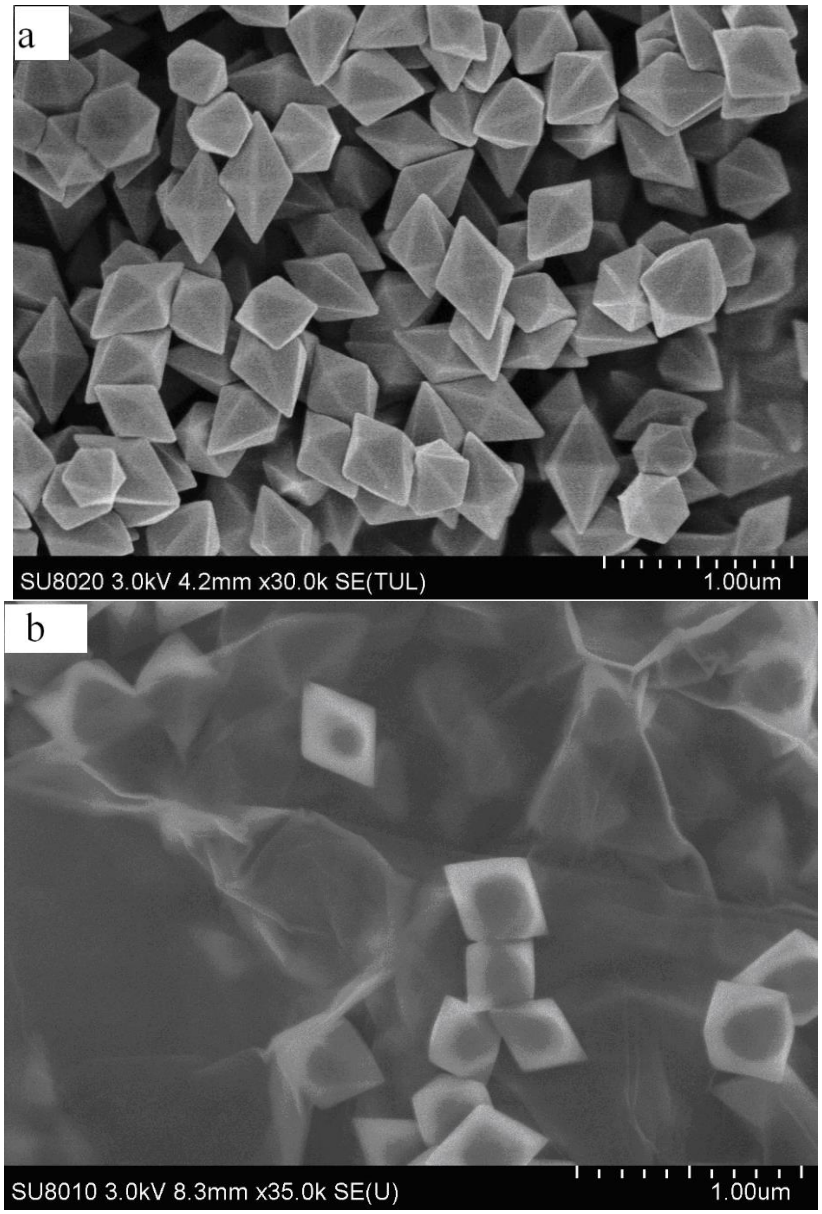

Figure 1. Typical SEM images of (a) the as-synthesized Fe-MOF crystals and (b) the Fe-MOF/rGO composite.

The Fe-MOF crystals were further examined by X-ray diffraction (XRD, Figure 2). The XRD pattern of Fe-MOF crystals showed strong and narrow peaks that are characteristic of Fe-MOF, indicating that the as-prepared sample had good crystallinity. The main peak positions of the Fe-MOF were in the range of 5-70°. Comparison of all the observed peaks taken from the experimental Fe-MOF sample with those of a previously reported XRD pattern demonstrates that the produced Fe-MOF sample had been successfully prepared [35].

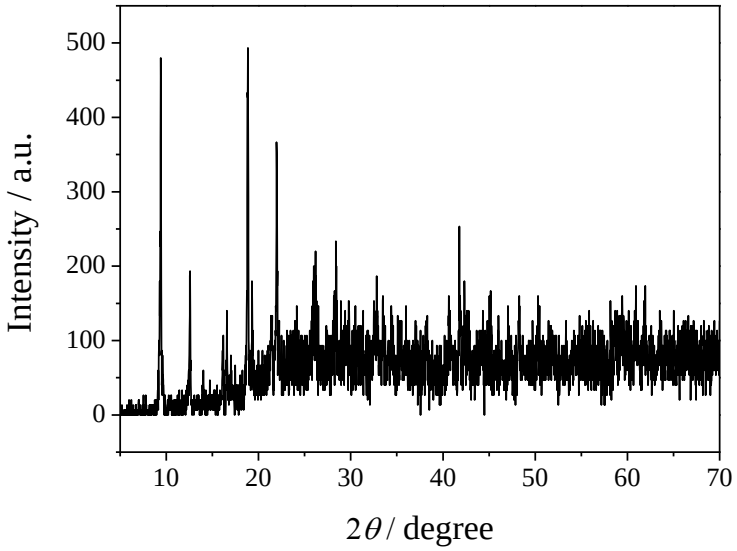

Figure 2. XRD pattern of the Fe-MOF crystals.

3.2 Electrochemical responses toward H_2O_2 for the different electrodes

Figure 3 shows the electrochemical responses of the different electrodes in 0.1 M pH 7.0 PBS containing 10.0 mM H_2O_2, which were obtained using cyclic voltammetry (CV), including Fe-MOF/rGO/CPE (curve a), rGO/CPE (curve b), Fe-MOF/CPE (curve c) and CPE (curve d). No detectable signal was observed for the bare CPE after the addition of H_2O_2, indicating the negligible electrocatalytic activity of the bare CPE (curve a) toward H_2O_2. However, in terms of rGO/CPE (curve b) and Fe-MOF/CPE (curve c), after the addition of 10.0 mM H_2O_2, an obvious increase in the current at negative potentials is observed, indicating that both rGO and Fe-MOF show electrocatalytic activity toward H_2O_2. When the two electrocatalysts are integrated together to form a Fe-MOF/rGO hybrid-material-modified electrode, remarkably high currents at negative potentials are obtained, which are the highest among all of the electrodes. According to the above observations, a possible electrochemical reaction mechanism can be proposed for H_2O_2 reduction on the Fe-MOF/rGO/CPE. In general, H_2O_2 may be reduced according to the following equation:

$$H_2O_2 + 2e^- + 2H^+ \rightarrow 2H_2O \quad (1)$$

The electrocatalytic mechanism of the Fe-MOF crystals can be proposed to be an electrochemical process as follows:

$$\text{Fe(III)-MOF} + e^- \rightarrow \text{Fe(II)-MOF} \quad (2)$$

$$\text{Fe(II)-MOF} + 2H_2O_2 \rightarrow \text{Fe(III)-MOF} + 2H_2O + O_2 \quad (3)$$

The reduction current for H_2O_2 can be increased on the surface of the Fe-MOF/rGO/CPE. This characteristic benefits from the existence of the highly regular six-angle bipyramidal structure of the Fe-MOF in the doped material, which can enhance the surface area. In addition, the existence of rGO in the Fe-MOF/rGO structure can improve the charge transfer ability of the modified electrode. Additionally, the enhanced catalytic activity may be attributable to a synergistic effect between the rGO and Fe-MOF.

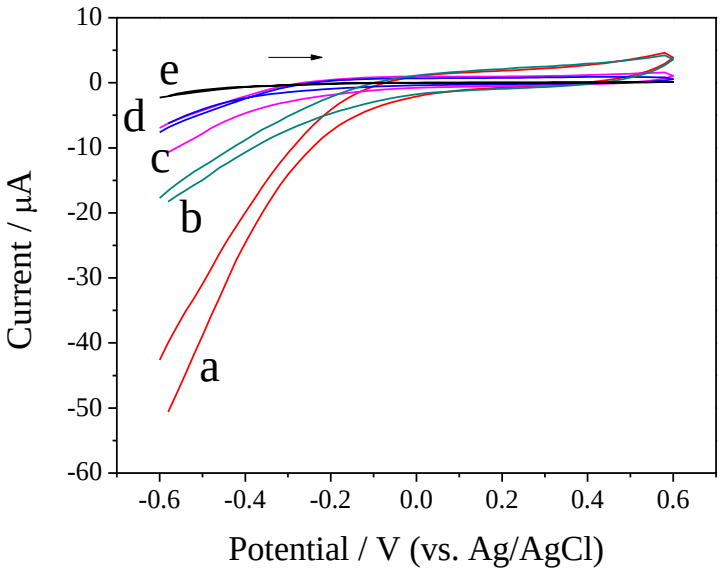

Figure 3. CVs of different electrodes: (a) Fe-MOF/rGO/CPE, (b) rGO, (c) Fe-MOF/CPE, (e) CPE in 0.1 M pH 7.0 PBS containing 10.0 mM H_2O_2 and (d) Fe-MOF/rGO/CPE in just 0.1 M pH 7.0 PBS; scan rate: 20 mV/s.

The current−time (*I*−*t*) responses were recorded to investigate the amperometric sensing properties of the different electrodes. The applied potential was −0.4 V. As shown in Figure 4, an amperometric response for the electrodes occurs within a short timeframe. Moreover, the current response of the Fe-MOF/rGO/CPE is substantially higher than those of the rGO/CPE, Fe-MOF/CPE and CPE. The Fe-MOF/rGO/CPE is the best electrode in this work, which loads the highly regular six-angle bipyramidal structure of the Fe-MOF within the rGO nanosheets, resulting in an exceptional electrocatalytic activity toward the reduction of H_2O_2.

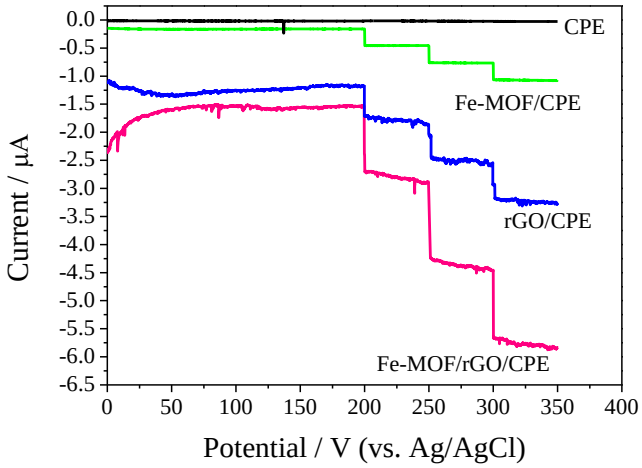

Figure 4. *I*–*t* curves of the different electrodes for three successive additions of 0.1 mM H_2O_2. The curves were measured in 0.1 M pH 7.0 PBS at an applied potential of −0.40 V.

3.3 Detection of H_2O_2

The rapid and sensitive H_2O_2 detection capabilities of the Fe-MOF/rGO/CPE were tested through the current–time responses upon successive injections of different amounts of H_2O_2 (Figure 5). At an applied potential of −0.4 V, the current response of the Fe-MOF/rGO/CPE decreases gradually with successive injections of H_2O_2 into the stirring PBS solution, and the response exhibits its maximum steady-state current within 5 s of injection.

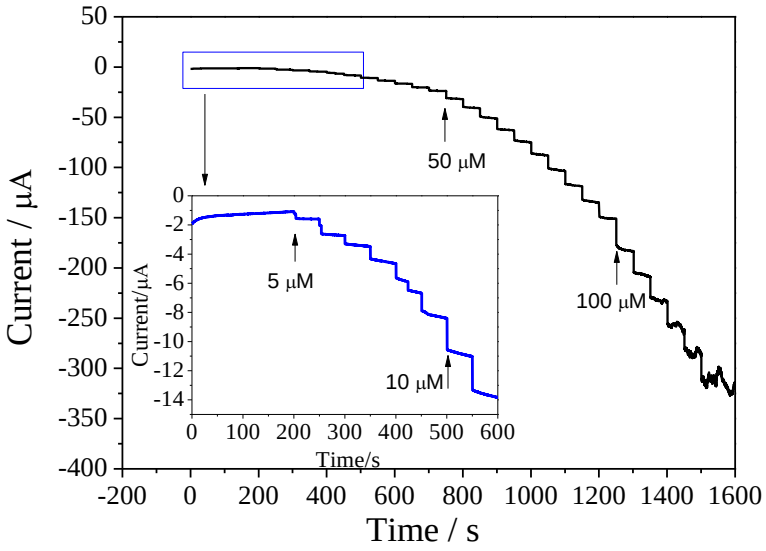

Figure 5. *I–t* curves of the Fe-MOF/rGO/CPE upon successive injections of different amounts of H_2O_2 into a stirring 0.1 M PBS (pH 7.0) solution at an applied potential of −0.4 V.

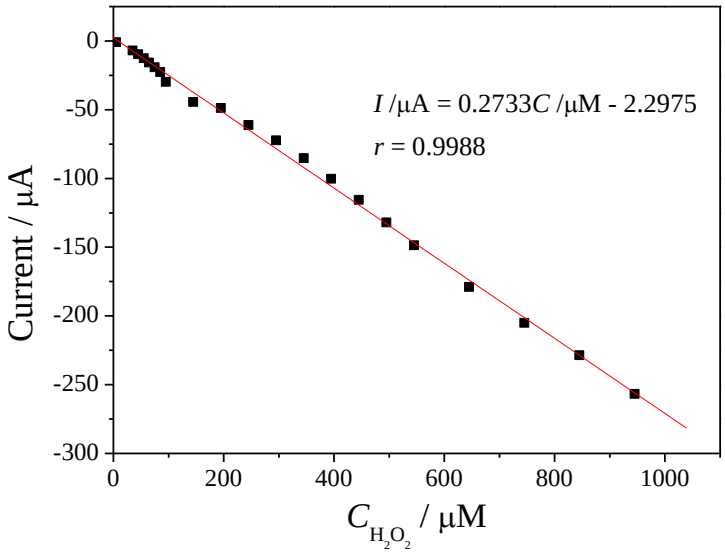

Figure 6. Relation of the response current toward H_2O_2 vs. H_2O_2 concentration in the range of 5–945 ìM.

The measured linear range of detection of the Fe-MOF/rGO/CPE (seen in Figure 6) spans the relatively broad H_2O_2 concentration range of 5.0 μM to 945 μM with a detection limit of 0.5 μM (S/N

= 3) and a detection sensitivity of 5.17 μA mM^{-1} cm^{-2}. Table 1 lists the comparative characteristics of the as-prepared sensor with those of previously reported sensors for the detection of H_2O_2. The obtained detection limit of H_2O_2 (0.5 μM) is lower than several MOF-based H_2O_2 sensors [3, 38, 39], graphene-based H_2O_2 sensors [40, 41], and biomolecule-based H_2O_2 sensors [42, 43]. Here, it is worth noting that Song et al [4]. prepared H_2O_2 sensors by combining sulfonated graphene with hemin, chitosan (CS), Cu-MOF and rGO. Although this biosensor demonstrated several excellent characteristics, the intrinsically biomolecular-based biosensor limits its widespread application due to the challenges in retaining the native stability and reaction activity of the biomolecule. However, in contrast, the H_2O_2 sensor constructed in this work displays several obvious advantages, such as a simple fabrication process, an excellent performance and a good electrocatalytic ability toward H_2O_2 without the aid of peroxide enzymes.

Table 1. Comparative characteristics of the as-prepared sensor and several reported sensors for the detection of H_2O_2.

Electrode material	Reduction potential	Linear range (ìM)	LOD (ìM)	Ref.
Cu-MOF	−0.2 V (Ag/AgCl)	1−900	1.0	[38]
Cr-MOF	−0.375 V (Ag/AgCl)	25−500 mM	3.52 mM	[3]
Co-MOF	−0.40 V (standard Hg/HgO)	5−9.0 mM	3.76 mM	[39]
Graphene/Cu_2O	−0.4 V (Ag/AgCl)	800−7800	20.8	[40]
Fe_3O_4/GO– PAMAM/Au	−0.2 V (Ag/AgCl)	0.2−1000	2	[41]
Cytc-HRP/ConA/HRP/MUA-MCH/Au	−0.05 V (SCE)	20−3000	7.83	[42]
Peroxidase/ionic liquid/Au/ titanate	−0.4 V (Ag/AgCl)	5−1000	2.1	[43]
Cu-hemin MOFs/CS-rGO	−0.175 V (SCE)	0.065−410	0.019	[4]
Fe-MOF/rGO	−0.4 V (Ag/AgCl)	5.0−945	0.5	This work

3.4 Reproducibility and stability

Under the optimized conditions, the reproducibility and stability of the Fe-MOF/rGO/CPE were studied. The same Fe-MOF/rGO/CPE electrode independently measured the same H_2O_2 solution 5 times, and the relative standard deviation (RSD) of the electrochemical response was 3.5%. These results reveal that the Fe-MOF/rGO/CPE had good reproducibility. Between measurements, the Fe-MOF/rGO/CPE was stored at room temperature. When used once per day, 97.5% and 90.6% of the

initial response of the Fe-MOF/rGO/CPE toward H_2O_2 remained after 1 and 5 days, respectively. These results indicate the excellent stability of the Fe-MOF/rGO/CPE.

3.5 Interference investigation

If the prepared sensor can be applied to analyze H_2O_2 in real samples, then it will be a meaningful device. Glycine, AA, glucose and UA are common molecules in physiological samples. An interference investigation was carried out by recording the amperometric response upon successive injection of glycine, AA, glucose, and UA, as shown in Figure 7. The Fe-MOF/rGO/CPE shows an obvious current response toward H_2O_2. With the successive additions of 10-fold excess of glycine, 50-fold excess of AA, 50-fold excess of UA and 100-fold excess of glucose, no obvious amperometric response is observed, according to a relative error of < ±15%, indicating that these species do not affect the detection of H_2O_2.

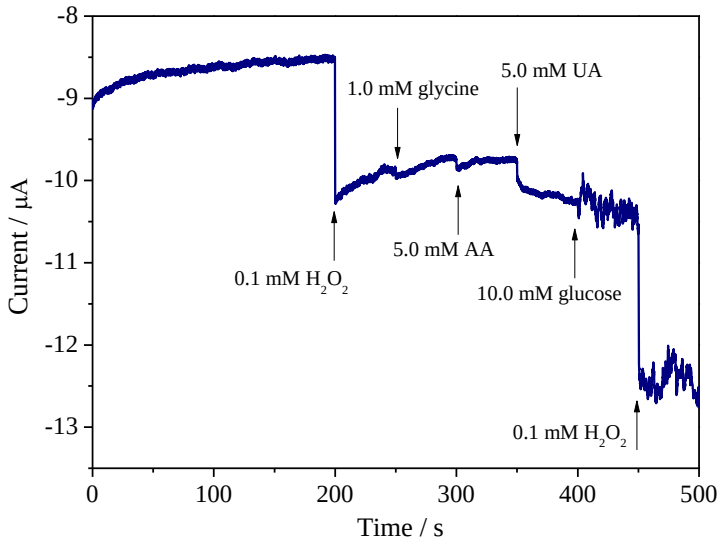

Figure 7. The amperometric response of the Fe-MOF/rGO/CPE to consecutive injections of 0.1 mM H_2O_2, 1.0 mM glycine, 5.0 mM AA, 5.0 mM UA, 10.0 mM glucose and 0.1 mM H_2O_2. Responses were measured in a 0.1 M pH 7.0 PBS solutions at an applied potential of −0.40 V.

3.6 Detection of H_2O_2 in a real sample

To further investigate the use of the sensor for practical analysis, the constructed sensor was applied to detect H_2O_2 in disinfectant samples without any pretreatment. The sample was injected into a stirring 0.1 M solution of N_2-saturated PBS (pH 7.0) and measured by a current-time curve. Moreover, the real sample was also measured by a H_2O_2 quantitative assay kit (water-compatible). The UV-Vis absorbance spectra were obtained on a UV-2700 spectrophotometer (Shimadzu), and the maximum absorption wavelength of 560 nm was used for the quantitative assay. A comparison of the results of the prepared electrode and the H_2O_2 quantitative assay kit is listed in Table 2. The results

indicate that there are no obvious differences between the two methods, demonstrating that the prepared sensor is reliable and can be used for real sample analysis.

Table 2. A comparison of the Fe-MOF/rGO/CPE and the H_2O_2 quantitative assay kit for the detection of H_2O_2 in a real sample.

Samples	By quantitative assay kit[a] (ìM)	By proposed method[a] (ìM)
1	20.00	20.08
2	40.21	39.47
3	60.30	59.62
4	79.86	78.78

[a] The values were obtained by averaging the values from four successive determinations.

4. CONCLUSION

In conclusion, a novel nanocomposite was developed comprising Fe-MOF with a highly regular six-angle bipyramidal structure doped onto rGO. The resulting Fe-MOF/rGO nanocomposite demonstrated a high electrocatalytic ability toward H_2O_2 reduction. Compared to known sensors of H_2O_2, the prepared electrode exhibits several interesting advantages: (i) simplicity of the preparation method for the direct crystallization of Fe-MOF; (ii) high sensitivity due to the large surface area, good electrocatalytic activity of Fe-MOF and electrical conductivity of graphene; (iii) excellent selectivity owing to the Fe-MOF; (iv) rapid response because of the inherent properties of Fe-MOF and rGO; and (v) good stability of the modified electrode. The results show that the Fe-MOF/rGO is a promising electrode material for application in electroanalysis, and it may introduce new methods to construct nonenzymatic electrochemical sensors that have excellent activity and high sensitivity.

ACKNOWLEDGEMENTS
The present work was supported by grants from the National Natural Science Foundation of China (NSFC, No. 21804002), the Program for Science and Technology Innovation Talents at the University of Henan Province (No. 18HASTIT005), Key scientific research projects in Henan colleges and Universities (No. 19A150016) and Anyang Science and Technology Bureau (No. 28).

SUPPLEMENTARY MATERIAL

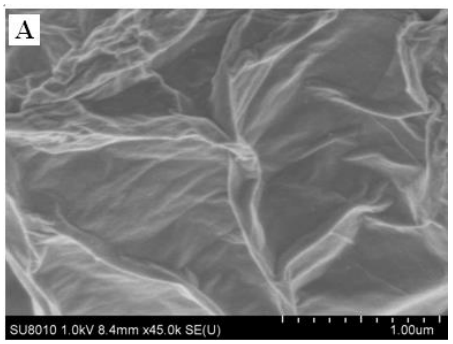

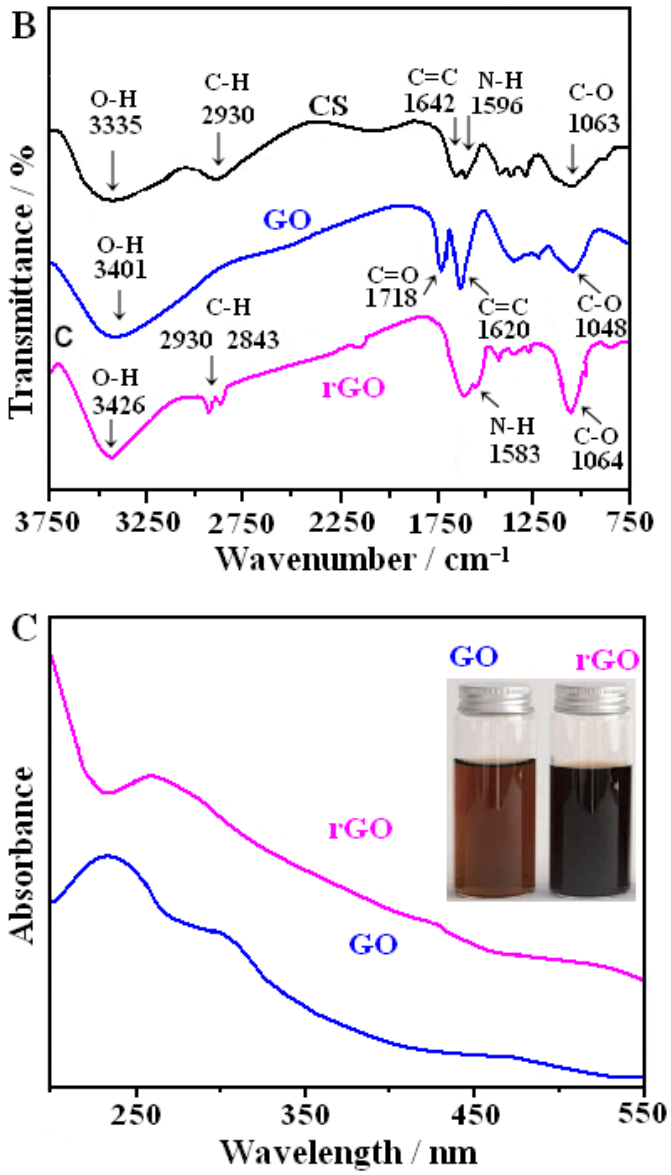

Figure S1. (A) SFM image of rGO; (B) FT-IR spectra of CS, GO and rGO; **(**C**)** UV-vis spectra of GO and rGO. Insets are the color change of GO suspension (yellow) and rGO suspension (black) after reduction.

Apparatus. The surface morphology were characterized with a field emission scanning electron microscopy (FE-SEM, JEOL 7401 F). UV-vis absorption spectra were recorded on a Lambda 35 UV-vis Spectrophotometer. Fourier transform-infrared (FT-IR) spectra were carried out on a Thermo Scientific Nicolet iS50 FTIR spectrometer (Thermo Fisher Scientific, USA).

Characterization of rGO

Typical SEM images of rGO was presented in Figure S1A. rGO showed wrinkled-shaped thin nanosheets, which was consistent with the previously reported GO. The result also demonstrated that the CS functionalized rGO had excellent dispersion.

FT-IR spectra (Figure S1B) were carried out to prove that GO was reduced by CS into rGO. The CS have peaks at 2930 cm^{-1} (ν_{C-H}), 1642 cm^{-1} ($\nu_{C=C}$) and 1063 cm^{-1} (ν_{C-O}) from the carbon skeleton of CS. The peaks at 3335 cm^{-1} and 1596 cm^{-1} were attributed to the –OH and $–NH_2$ groups on macromolecular chains of CS, and the groups can form electrostatic interactions with the GO and

reduce it under high temperature. At FT-IR spectrum of rGO, the stretching vibrations in carboxylic acid at 1718 cm^{-1} ($\nu_{C=O}$) disappeared and N-H bending vibration due to amide II band at 1583cm-1 obtained, which showed that GO was successfully reduced by CS and realized functionalized rGO.

UV-vis spectra were monitored to further verify the synthesis process (Figure S1C). GO expressed two strong absorption peaks at 232 nm and 305 nm, corresponding to $\pi \rightarrow \pi^*$ transitions of C=C band and $n \rightarrow \pi^*$ transitions of C=O band, respectively. After GO was reduced by CS, π-π^* of C=C red shifted at 264 nm and the absorption peak at 300 nm for n-π^* of C=O disappeared. All the results confirmed that CS functionalized rGO was obtained. Inset of Figure S1C exhibited the color change of GO suspension from yellow to black after the reduction. It is noteworthy that the dispersion of CS functionalized rGO is very stable.

References

1. Y. Zhou, C. Li, Y. Hao, B. Ye and M. Xu, *Talanta,* 188 (2018) 282.
2. R. Zhang and W. Chen, *Biosens. Bioelectron.,* 89 (2017) 249.
3. N.S. Lopa, M.M. Rahman, F. Ahmed, S. Chandra Sutradhar, T. Ryu and W. Kim, *Electrochim. Acta,* 274 (2018) 49.
4. L. Wang, H. Yang, J. He, Y. Zhang, J. Yu and Y. Song, *Electrochim. Acta,* 213 (2016) 691.
5. M.R. Zhang, X.Q. Chen and G.B. Pan, *Sens. Actuators B,* 240 (2017) 142.
6. J. Li, H. Hu, H. Li and C. Yao, *J. Mater. Sci.,* 52 (2017) 10455.
7. Y.Y. Zhang, X.Y. Bai, X.M. Wang, K.K. Shiu, Y.L. Zhu and H. Jiang, *Anal. Chem.,* 86 (2014) 9459.
8. Y. Sun, M. Luo, X. Meng, J. Xiang, L. Wang, Q. Ren and S. Guo, *Anal Chem.,* 89 (2017) 3761.
9. L.L. Tian, K.D. Xia, W.P. Hu, X.H. Zhong, Y.L. Chen, C. Yang, G.G. He, Y.Y. Su and L. Li, *Electrochim. Acta,* 231 (2017) 190.
10. S. Berbeć, S. Żołądek, A. Jabłońska and B. Pałys, *Sens. Actuators B,* 258 (2018) 745.
11. J. Bai, C. Sun and X. Jiang, *Anal Bioanal Chem.,* 408 (2016) 4705.
12. C. Peng, S. Zhou, X. Zhang, T. Zeng, W. Zhang, H. Li, X. Liu and P. Zhao, *Sens. Actuators B,* 270 (2018) 530.
13. K. Vijayalakshmi, A. Renitta, K. Alagusundaram and A. Monamary, *Mater. Chem. Phys,* 214 (2018) 431.
14. Y. Zheng, Z. Wang, F. Peng and L. Fu, *Braz. J. Pharm. Sci.,* 52 (2016) 781.
15. C. Zhang, M. Wang, L. Liu, X. Yang and X. Xu. *Electrochem. Commun.,* 33 (2013) 131.
16. B. Sherino, S. Mohamad, S.N.A. Halim and N.S. Abdul. Manan, *Sens. Actuators B,* 254 (2018) 1148.
17. Z. Liang, C. Qu, D. Xia, R. Zou and Q. Xu, *Angew. Chem. Int. Ed.,* 57 (2018) 4891.
18. S. L. James, *Chem. Soc. Rev.,* 32 (2003) 276.
19. A. Dhakshinamoorthy, A. M. Asiri and H. García, *Angew Chem Int Ed Engl.,* 55 (2016) 5414.
20. X. Chen, R. Tong, Z. Shi, B. Yang, H. Liu, S. Ding, X. Wang, Q. Lei, J. Wu and W. Fang, *ACS Appl. Mater. Interfaces,* 10 (2018) 2328.
21. C.Y. Gao, H.R. Tian, J. Ai, L. J. Li, S. Dang, Y.Q. Lan and Z.M. Sun, *Chem Commun (Camb).,* 52 (2016) 11147.
22. D.Y. Ahn, D.Y. Lee, C.Y. Shin, H.T. Bui, N.K. Shrestha, L. Giebeler, Y.Y. Noh and S.H. Han, *ACS Appl. Mater. Interfaces,* 9 (2017) 12930.
23. K. M. Choi, J. H. Park and J. K. Kang, *Chem. Mater.,* 27 (2015) 5088.
24. Z. Song, N. Cheng, L. Andrew and X. Sun, *Catalysts,* 6 (2016) 1.
25. Y. Zhang, X. Bo, C. Luhana, H. Wang, M. Li and L. Guo, *Chem. Commun.,* 49 (2013) 6885.
26. P. Arul and S. Abraham John, *Electrochim. Acta,* 235 (2017) 680.
27. Y. Shu, Y. Yan, J. Chen, Q. Xu, H. Pang and X. Hu, *ACS Appl. Mater. Interfaces,* 9 (2017) 22342.

28. M. S. Rahmanifar, H. Hesari, A. Noori, M. Y. Masoomi, A. Morsali and M. F. Mousavi, *Electrochim. Acta*, 275 (2018) 76.
29. L. Liu, Y. Yan, Z. Cai, S. Lin and X. Hu, *Adv. Mater. Interfaces*, 5 (2018) 1701548.
30. F. Zhang, L. Liu, X. Tan, X. Sang, J. Zhang, C. Liu, B. Zhang, B. Han and G. Yang, *Soft Matter.*, 13 (2017) 7365.
31. C. Petit and T. J. Bandosz, *Adv. Mater.*, 21 (2009), 4753.
32. M. Jahan, Q. Bao and K. P. Loh, *J. Am. Chem. Soc.*, 134 (2012) 6707.
33. X. Cao, B. Zheng, X. Rui, W. Shi, Q. Yan and H. Zhang, *Angew. Chem., Int. Ed.*, 53 (2014) 1404.
34. X. Ge, Z. Li and L. Yin, *Nano Energy*, 32 (2017) 117.
35. X. Xu, W. Shi, P. Li, S. Ye, C. Ye, H. Ye and T. Lu, *Chem. Mater.*, 29 (2017) 6058.
36. W.S. Hummers and R.E. Offeman, *J. Am. Chem. Soc.*, 80 (1958) 1339.
37. Y.H. Song, H.Y. Liu, H.L. Tan, F.G. Xu, J.B. Jia, L.X. Zhang and Z. Li, L. Wang, *Anal. Chem.*, 86 (2014) 1980.
38. D. Zhang, J. Zhang and R. Zhang, *Talanta*, 144 (2015) 1176.
39. L. Yang, C. Xu, W. Ye and W. Liu, *Sens. Actuators B*, 215 (2015) 489.
40. M. Liu, R. Liu and W. Chen, *Biosens. Bioelectron.*, 45 (2013) 206.
41. X. Yang, L. Wang, G. Zhou, N. Sui, Y. Gu and J. Wan, *J. Clust. Sci.*, 26 (2014) 1.
42. Y. Song, Y. Wang， H. Liu and L. Wang, *Int. J. Electrochem. Sci.*, 7 (2012) 11206.
43. X. Liu, H. Feng, R. Zhao, Y. Wang and X. Liu, *Biosens. Bioelectron.*, 31 (2012) 101.

© 2019 The Authors. Published by ESG (www.electrochemsci.org). This article is an open access article distributed under the terms and conditions of the Creative Commons Attribution license (http://creativecommons.org/licenses/by/4.0/).